2003

A deterministic interfacial cyclic oxidation spalling model

James L. Smialek
NASA Glenn Research Center, james.l.smialek@nasa.gov

Available online at www.sciencedirect.com
SCIENCE DIRECT®
Pergamon
Acta Materialia 51 (2003) 469–483
Acta MATERIALIA
www.actamat-journals.com

A deterministic interfacial cyclic oxidation spalling model

James L. Smialek

Materials Division, NASA Glenn Research Center, 21000 Brookpark Rd., Cleveland, OH 44135, USA

Received 16 April 2002; received in revised form 13 September 2002; accepted 13 September 2002

Abstract

A series summation has been developed to model the iterative scale growth and spalling process of cyclic oxidation. Parabolic scale growth has been assumed. Interfacial spallation of a constant area fraction was stipulated to occur only at the thickest portions. Inputs are the parabolic growth rate constant, spall area fraction, oxide stoichiometry, and cycle duration. Outputs include the net weight change, amount of oxygen and metal consumed, and amount of oxide spalled. Classic weight change curves are produced with an initial maximum and final linear weight loss rate. This simplicity allowed for representation by explicit algebraic functions for all outputs and characteristic features. The maximum in weight change varies directly with the parabolic rate constant and cycle duration and inversely with the spall fraction, all to the $^{1}/_{2}$ power. The ratio of the number of cycles to reach maximum and zero weight change is exactly 1:3, and these vary only with the inverse of the spall fraction. Many similarities to and some differences with previous cyclic models are identified.
Published by Elsevier Science Ltd on behalf of Acta Materialia.

Keywords: Thermal cycling; Oxidation; Modeling; Kinetics; Nickel alloys

1. Introduction

Oxidation is an important degradation process for high temperature materials operating in air or oxygen. For isothermal exposures, the rate of oxidation determines the rate of material consumption. Both are generally controlled by solid state diffusion through the scale layer and show approximately parabolic kinetics in which the instantaneous rate is inversely proportional to the existing scale thickness. Many components, however, experience cyclic oxidation in applications that entail periodic start-up and shutdown. Typically, some scale spallation may occur upon cooling, resulting in loss of the protective diffusion barrier provided by a fully intact scale. Upon reheating, the component will therefore experience accelerated oxidation in the spalled regions because of the inverse growth rate dependence upon thickness.

Cyclic oxidation testing has therefore been a mainstay of material characterization and performance ranking for high temperature materials. The engineering response is generally characterized nondestructively by weight change curves and surface recession. A general trend of surface recession can be linked with an empirical cyclic oxidation weight change ‘attack parameter’, which takes into

E-mail address: james.l.smialek@grs.nasa.gov (J.L. Smialek).

1359-6454/03/$30.00 Published by Elsevier Science Ltd on behalf of Acta Materialia.
doi:10.1016/S1359-6454(02)00430-5

Nomenclature

i	oxide segment index
j	number of oxidation cycles
j_{max}	cycle number to reach maximum weight gain
j_o	cycle number to reach zero weight change
$(\Delta W/A)$	specific weight change (mg/cm^2)
$(\Delta W/A)_{max}$	maximum in cyclic oxidation weight change curve, (mg/cm^2)
n_o	number of oxide segments
F_a	spall area fraction constant=$1/n_o$
k_p	parabolic growth rate (mg^2/cm^4 h)
t	total heating time (h)
Δt	heating cycle duration (h)
S_c	stoichiometric constant, weight fraction of oxide/oxygen
W_r	weight of oxide retained after cooldown (mg/cm^2)
W'_r	weight of oxide retained before cooldown (mg/cm^2)
ΣW_{met}	cumulative amount of metal consumed (mg/cm^2)
ΣW_{oxy}	cumulative amount of oxygen consumed (mg/cm^2)
ΣW_{spall}	cumulative amount of oxide spalled (mg/cm^2)
F_s	weight fraction of oxide spalled
TS	terminal slope of weight change curve

account degradation by both scale growth and spallation [1]. However, a direct quantitative relationship between cyclic weight change and material degradation (i.e., metal consumed) is not normally measured.

One important step toward approaching this direct relationship has been the development of mathematical cyclic oxidation spalling models that simulate the discreet processes that occur each time the scale spalls upon cooling and re-grows upon heating. In general, a scale growth law is postulated with a fixed rate constant, and a spalling formalism is defined which dictates the type and amount of spalling that occurs each cycle. This unit process is formally described by means of summation series or an algorithm, by which an iterative calculation may generate the entire cyclic oxidation curve. The former has been done for the case of interfacial spalling, where a constant area fraction of each portion of the scale has been proposed to spall each cycle [2].

The latter has been developed for the case where a uniform external layer of specified thickness spalls off the entire area (i.e., no discrete segments). Here the fractional thickness that spalls is a direct function of the existing scale thickness [3]. This spalling criterion has been further modified to allow for non-uniform or bimodal spallation, in which some portions do not spall at all on a given cycle, while others spall some fixed ratio of the thickness - including the possibility of total interfacial spallation [4]. The consolidated package, termed COSP (Cyclic Oxidation Spalling Program, available for DOS and Windows 95, 98, and 2000 [4,5]), allows for the selection of various scale growth laws, spalling functions, and spalling configurations.

Families of model curves exhibit consistent regularity and trends with input parameters, and characteristic features have been empirically described in terms of these inputs [2,4,5,7]. However, precise mathematical dependencies of these trends have eluded derivation. Indeed, the model cyclic weight change curve itself cannot be obtained analytically, but relies totally upon series summations or iterative calculations.

These models can describe cyclic oxidation results when a reasonable fit has been obtained

through adjusting the various input parameters. The utility of such fitted curves is the ability to predict long-term behavior, assuming that no mechanistic changes take place. Another value is the ability to extract the amount of metal consumed as the most direct figure of merit regarding material degradation. Coupled with diffusion models, solute depletion and the transition to non-protective oxidation behavior may be predicted for coatings and alloys [6]. (Related issues have been presented in a recent summary paper [7], along with many other pertinent high temperature cyclic oxidation topics [8].)

While independent measurements of the growth rate have generally agreed with the growth rates obtained from model fits, there is less successful verification or prediction of the amount of scale that should spall each cycle. At best, it has been observed experimentally that the relative amount of spalling increases with scale thickness. These conclusions were made by both weight change and surface area measurements [2,3]. However, the actual thickness and area of the spalled segments has not been determined.

Ideally, fracture mechanics could address the critical stress in the scale and the type and degree of spallation that occurs each cycle. Compressive thermal expansion mismatch stress is commonly accepted as the primary cause of spallation and is additive to any growth stresses that are retained after cooldown. Scale spallation has been defined as a buckling instablility or wedge-driven crack growth in an extensive review [9]. The growth and thermal stresses generated in protective alumina scales have been elegantly and thoroughly studied through the use of photo-stimulated luminescence (piezospectroscopy) [10]. Furthermore , the size of a spall segment has been modeled from the strain energy in the scale, the scale thickness, and interfacial toughness. [11,12]. These studies are leading the way to postulate the morphology and quantity of spalling.

Ultimately, the relationship between cyclic weight change (scale spallation) and mechanics-based approaches may be drawn, as controlled by scale (or interface) fracture toughness [13] or stored strain energy [14]. Both approaches met with good success, although these fitted parameters were not independently generated. Therefore, at the present time, empirical fitting remains the primary means by which a cyclic oxidation weight change curve is modeled.

The purpose of the present paper is to present the development of a simple model simulation that assumes interfacial spallation to the bare metal surface every cycle. Furthermore, this spallation is biased toward the thickest oxide regions that have yet to spall, as would be suggested by the previous analyses [2–14], but does not stipulate that a critical oxide thickness be attained as a spalling criterion. Some of these features have been observed on commercial NiAl and occasionally Ni(Pt)Al bond coatings, as well as on uncoated single crystal superalloys [15–17]. The model simplicity propagates into the mathematical formulations, allowing for more transparent relationships between input and outputs. Finally, through a mathematical simplification, the cyclic oxidation curve is completely described by simple algebraic functions.

2. Model development

2.1. Weight change equations.

According to basic diffusional models of oxidation, a scale will grow with parabolic kinetics, such that the sample weight (mass) gain per unit area, $\Delta W/A$, is given by

$$\Delta W/A = \sqrt{k_p t} \tag{1}$$

for rate constant k_p and heating duration t (see Nomenclature for a full glossary of symbols). According to this definition of k_p, the weight change upon heating reflects only the weight gain of the ***oxygen*** reacted. Upon cooling, spalling may take place, which will reflect the weight of the ***oxide*** segment lost (metal+oxygen). (Note that the term *weight* gain and loss are being used according to a common convention, rather than *mass*).

Description of the spalling mode requires more detailed specification. The present simple model assumes a constant area fraction, F_A, will spall to the bare metal surface each cycle. The sample can be viewed to be divided up into n_o equivalent segments, where $n_o=1/F_A$, and each of these segments

will have its own individual oxide growth and spallation history. These segments, with fractional area (F_A) and with thickness (or weight) proportional to the square root of its growth interval, will be the basic cells in constructing the model.

2.1.1. Case A: primary spallation sequence

In Fig. 1, a schematic cross-section of the oxidized surface is shown for the case where the area spall fraction F_A=0.1 and thus n_o=10 segments. Here, the growth and spalling sequence of each *i*th segment is presented for the first five cycles (j=1–5). For the sake of simplicity, the height of each oxide segment is represented only by its corresponding growth time. After one cycle, the entire surface has grown a scale according to Eq. (1) (above the zero-growth line) and one segment corresponding to one time unit has spalled (below the line). After two cycles, the first segment (i=1) has re-grown to a thickness of $\sqrt{k_p\Delta t}$. All the remaining second segments (i=2–10), have grown to$\sqrt{k_p 2\cdot\Delta t}$, but the second segment has now spalled. (That is, while each segment is illustrated in terms of equal cycle time units, it is understood that the actual segment weight is proportional to the square root of its total growth time.)

Single spalled segments adjacent to that of the previous cycle are indicated here for visual simplicity, but this is not required by the mathematics or in practice. Rather, any dispersion of any number of discrete spalled regions may be represented by the model, as long as the total spalled area equals that of the model 'segment'. Implicit in the spalling sequence is that the next segment to spall is **always** the thickest segment (or as thick as any other equivalent segments). While, there is no critical thickness at which spallation begins, the effects are felt progressively as the scale thickens.

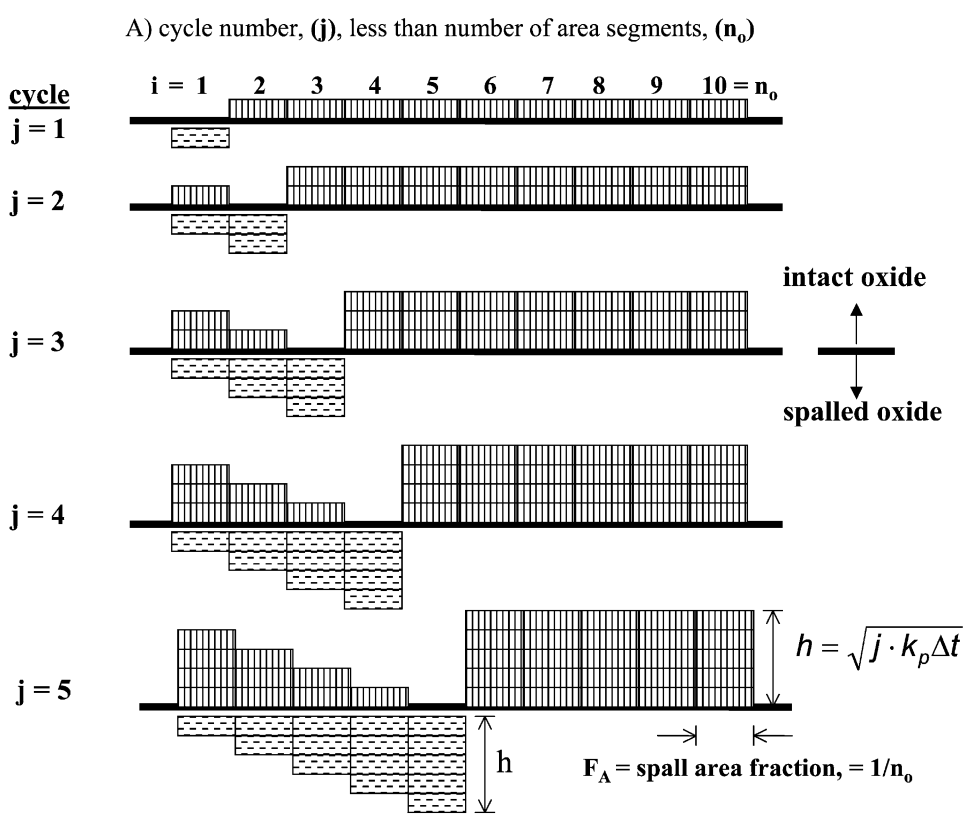

Fig. 1. Schematic cross-section of intact and spalled oxide segments (above and below the line) for the first five cycles of oxide growth and spallation. Case A: $j<n_o$. Each block corresponds to a basic unit area, F_A, and growth interval, Δt.

In general, the weight **gain** (segment height) of oxide remaining in each intact segment is given by:

$$(\Delta W/A)_{i,j,\ \text{intact}} = \sqrt{j \cdot k_p \Delta t} \tag{2}$$

where $(n_o - j)\cdot F_A$ is the relative area of the intact portion. Again, weight gain reflects only the amount of oxygen in the segments, implicit in the definition of k_p.

However, the amount of weight **loss** due to spallation must take into account the weight of metal in the oxide. The weight of oxide relative to that of oxygen is given by a stoichiometric constant, S_c, defined as the molecular weight ratio of oxide to oxygen in any given oxide, e.g., Al_2O_3, Cr_2O_3, NiO, etc. Oxide weight is obtained by multiplying the corresponding oxygen weight by S_c, and the amount of metal in a given segment is obtained by multiplying by $(S_c - 1)$.

By examination of these schematics or use of simplifying notations [18], the weight gain of the left-most segments that have spalled once and regrown new oxide for the time interval elapsed after spallation is seen to be:

$$F_A \sum_{i=1}^{j-1} \sqrt{(j-i)\cdot k_p \Delta t} \tag{3}$$

The weight gain of all the intact right-most segments is given by:

$$(n_o - j) F_A \sqrt{j \cdot k_p \Delta t} \tag{4}$$

Finally, the weight change due to just the metal lost in the spalled segments is given by:

$$-(S_c - 1) F_A \left\{ \sum_{i=1}^{j} \sqrt{i \cdot k_p \Delta t} \right\} \tag{5}$$

The same sequence of growth and spallation can be envisioned to occur here for up to 10 cycles ($j \le n_o$, case A), at which time the entire surface would have spalled just one time, and the number of cycles, j, is just equal to the number of segments, n_o.

2.1.2. Case B: secondary and subsequent spallation sequences

For $j \ge n_o$, continued spallation produces a modification in the sequence. At j=11, the first segment is now the thickest segment (corresponding to 10 Δt) and is sequenced for its second spallation event, as shown in Fig. 2. At j=12, the second segment spalls, also 10 time units thick. All subsequent spall segments will correspond to this maximum of 10 units (i.e., $n_o \cdot \Delta t$). Thus, for visual simplicity and convenience, these secondary spall segments are all shown as solid blocks, with a weight loss equivalent of $(S_c - 1)\sqrt{k_p 10 \cdot \Delta t}$.

The continued progression of this secondary spall sequence leads to the observation that the total amount of retained scale remains the same, even though the thickness over each particular area segment changes each cycle. The oxygen gain obtained from all the growth segments above the zero-growth line is thus given by an invariant quantity [18]:

$$F_A \sum_{i=1}^{n_o - 1} \sqrt{i \cdot k_p \Delta t} \tag{6}$$

Similarly, the metal loss due to the first series of spalled segments is invariant and is given by:

$$-(S_c - 1) F_A \left\{ \sum_{i=1}^{n_o} \sqrt{i \cdot k_p \Delta t} \right\}, \tag{7}$$

while the series of the secondary spall segments produces the term:

$$-(S_c - 1)\cdot(j - n_o) F_A \sqrt{n_o \cdot k_p \Delta t} \tag{8}$$

By combining all the appropriate oxygen gain and metal loss terms and simplifying the summations, the following relationships are obtained describing cyclic oxidation net weight change according to this model:

For cycle number $j \le n_o$ (Case A):

$$(\Delta W/A)_A = F_A \sqrt{k_p \Delta t} \left\{ (2 - S_c) \sum_{i=1}^{j} \sqrt{i} + (n_o - j - 1)\sqrt{j} \right\} \tag{9}$$

And for cycle number $j \ge n_o$ (Case B):

$$(\Delta W/A)_B = F_A \sqrt{k_p \Delta t} \left\{ (2 - S_c) \sum_{i=1}^{n_o} \sqrt{i} + [(1 - S_c)(j - n_o) - 1]\sqrt{n_o} \right\} \tag{10}$$

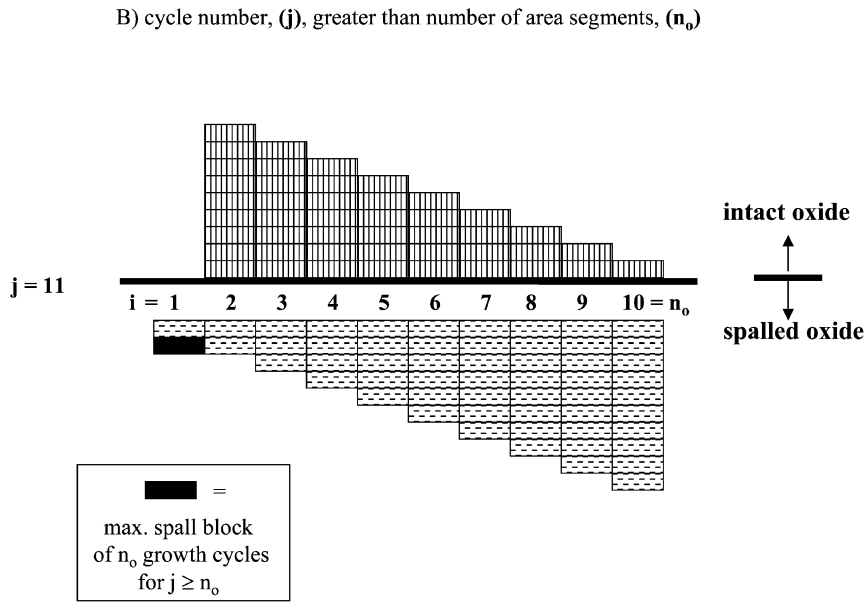

Fig. 2. Schematic cross-section of intact and spalled oxide segments (above and below the line) after the first 11 cycles of oxide growth and spallation. Case B: $j>n_o$. Each block corresponds to a basic unit area, F_A, and growth interval, Δt.

Consequently, two relationships (for Case A and B), are applied when the number of cycles, j, is less than or greater than the number of segments, n_o, to construct a full deterministic interfacial cyclic oxidation spalling model (DICOSM) weight change curve.

An example of a net weight change curve is shown in Fig. 3 for the following input parameters: k_p=0.01 mg^2/cm^4 h, Δt=1.0 h, F_A=0.001 (i.e., n_o=1000), and S_c=2.0, for j up to 2000 h. The classic shape and the general characteristics of a cyclic oxidation weight change curve are produced. Here the response follows parabolic growth initially, gradually degrading by spallation, then produces a maximum and eventually negative values. When $j=n_o$, i.e., 1000, a steady state, linear rate of weight loss is obtained and continues indefinitely according to the sequencing example in Fig. 2 and Eq. (10), i.e., Case B. In reality, excessive solute depletion may eventually cause a critical composition to be reached that triggers a mechanism change.

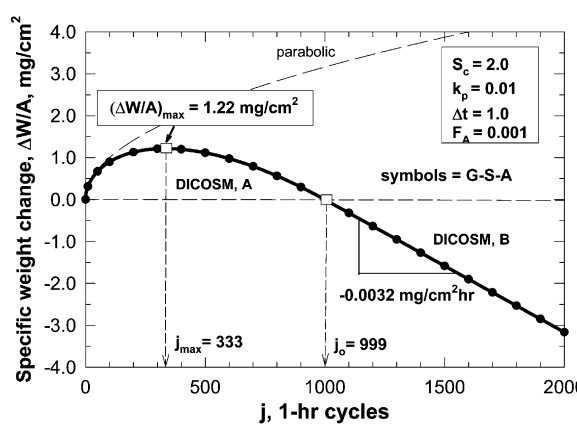

Fig. 3. DICOSM model curve of specific weight change vs cycle time for the parameters k_p=0.01 mg^2/cm^4 h, Δt=1.0 h, F_A=0.001 (i.e., n_o=1000), and S_c=2.0. Solid line, exact model calculation; solid circles, Good–Smialek approximation.

2.2. Other outputs

While the weight change curve represents the most commonly measured value in practice, there are other terms that describe a number of significant aspects of the cyclic oxidation process. Some of these additional terms may also be easily obtained from the DICOSM model described in Figs. 1 and 2, as listed below [18]:

- Total amounts of oxygen and metal reacted
- Weight of retained oxide immediately before and after spallation
- Total amount of oxide spalled
- Fractional amount of oxide spalled per cycle

Relations for most of these terms are listed in Table 1. Unfortunately, there are usually two equations for each, again depending on whether or not $j>n_o$. The total amount of oxygen reacted, $\Sigma W_{oxy,A}$, for Case A can be determined from inspection of Fig. 1 using the terms (3)–(5), but without the contribution of the metal stoichiometric factor (S_c-1). The same is true for Case B, using terms (6)–(8) along with Fig. 2. The metal reacted for both cases is simply the amount of oxygen reacted multiplied by (S_c-1).

The oxide retained after spalling, W_r, corresponds to the weight of oxygen in all the intact growth segments (above the line) multiplied by S_c. Thus for Case A, the segments described by the terms in (3) and (4) apply, but must be multiplied by the stoichiometric factor, S_c. For Case B, the segments in term (6) applies. The oxide retained just before cooling (spalling), W'_r, is obtained by adding the weight of the last spall segment to W_r.

The total amount of oxide spalled for Case A and B can be obtained from the series in terms (5) and (7) and (8), respectively, to account for all the segments below the line, but multiplied by S_c. Finally, the fraction of oxide spalled on any given cycle is given by the weight of the current spall segment divided by that of the total amount of retained oxide just before spallation (cooldown), W'_r. That is, the spalled segment after the jth cycle, with a weight given by $F_A\sqrt{j\cdot k_p\Delta t}$ (Case A) or $F_A\sqrt{n_o\cdot k_p\Delta t}$ (Case B), should be divided by $W'_{r,A}$ or $W'_{r,B}$, respectively.

Table 1
List of relationships describing DICOSM model outputs

Total amounts of oxygen and metal reacted:

$$\sum W_{oxy,A} = F_A\sqrt{k_p\Delta t}\left\{2\sum_{i=1}^{j}\sqrt{i} + (n_o-j-1)\sqrt{j}\right\}$$

$$\sum W_{oxy,B} = F_A\sqrt{k_p\Delta t}\left\{2\sum_{i=1}^{n_o}\sqrt{i} + (j-n_o-1)\sqrt{n_o}\right\}$$

$$\sum W_{met} = (S_c-1)\sum W_{oxy}$$

Amount of scale retained before and after spallation:

$$W'_{r,A} = S_cF_A\sqrt{k_p\Delta t}\left\{\sum_{i=1}^{j}\sqrt{i} + (n_o-j)\sqrt{j}\right\}$$

$$W_{r,A} = S_cF_A\sqrt{k_p\Delta t}\left\{\sum_{i=1}^{j}\sqrt{i} + (n_o-j-1)\sqrt{j}\right\}$$

$$W'_{r,B} = S_cF_A\sqrt{k_p\Delta t}\left\{\sum_{i=1}^{n_o}\sqrt{i}\right\}$$

$$W_{r,B} = S_cF_A\sqrt{k_p\Delta t}\left\{\sum_{i=1}^{n-1}\sqrt{i}\right\}$$

Total and fractional amounts of scale spalled:

$$\sum W_{s,A} = S_cF_A\sqrt{k_p\Delta t}\left\{\sum_{i=1}^{j}\sqrt{i}\right\}$$

$$\sum W_{s,B} = S_cF_A\sqrt{k_p\Delta t}\left\{\sum_{i=1}^{n_o}\sqrt{i} + (j-n_0)\sqrt{n_o}\right\}$$

$$F_{s,A} = \frac{\sqrt{j}}{\sum_{i=1}^{j}\sqrt{i} + (n_o-j)\sqrt{j}}$$

$$F_{s,B} = \frac{\sqrt{n_o}}{\sum_{i=1}^{n_o}\sqrt{i}}$$

These other outputs are plotted in Fig. 4 for the same model conditions as those in Fig. 3. The oxygen and metal reacted follow similar trends as might be expected. However, in this special case where S_c=2, these quantities are actually identical and equal to 1. The amount of retained oxide follows a gradual gain and becomes constant at $j=n_o$. The amount of oxide spalled follows a gradually increasing rate that becomes a constant at $j=n_o$. The fractional amount of oxide spalled also follows an increasing rate then levels at $j=n_o$ to ~3/2 F_A, as will be shown later.

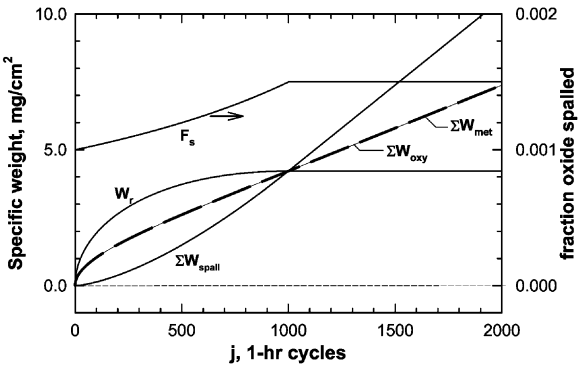

Fig. 4. Other DICOSM model outputs (total amount of oxygen and metal reacted, amount of retained scale and fraction of scale spalled, total amount of spalled scale) vs cycle time for the parameters k_p=0.01 mg^2/cm^4 h, Δt=1.0 h, F_A=0.001 (i.e., n_o=1000), and S_c=2.0.

3. Effects of model inputs

Characteristic trends in model weight change curves occur as the input parameters are varied, Figs. 5–7. A common baseline curve (S_c=2.0, k_p=0.01 mg/cm^2 h, F_A=0.001, and Δt=1 h) is always presented for comparison. The range of parameters addressed was chosen to illustrate effects in the region of ±5 mg/cm^2 over about 1000 h, corresponding to the behavior of many oxidation resistant materials.

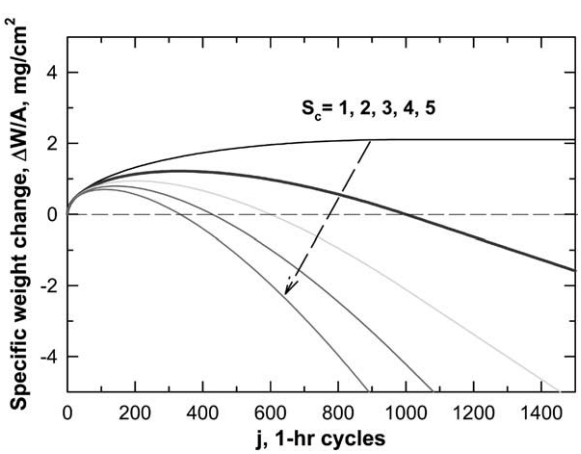

Fig. 5. The effect of the stoichiometric constant, S_c, on the family of DICOSM weight change curves. Baseline value of S_c=2.0 shown as bold line (k_p=0.01 mg^2/cm^4 h, Δt=1.0 h, F_A=0.001).

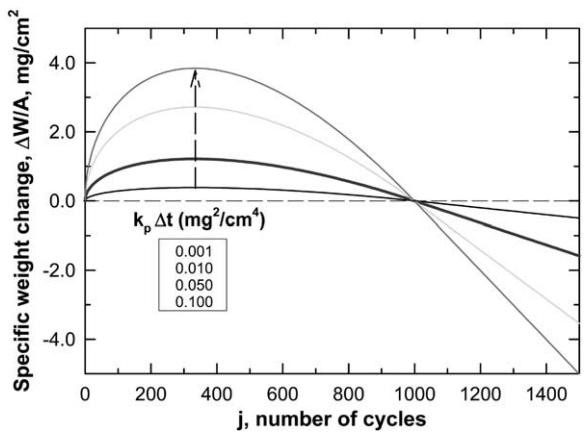

Fig. 6. The effect of the growth product, $k_p\Delta t$, on the family of DICOSM weight change curves. Baseline value of $k_p\Delta t$=0.01 mg^2/cm^4 shown as bold line (S_c=2.0, F_A=0.001).

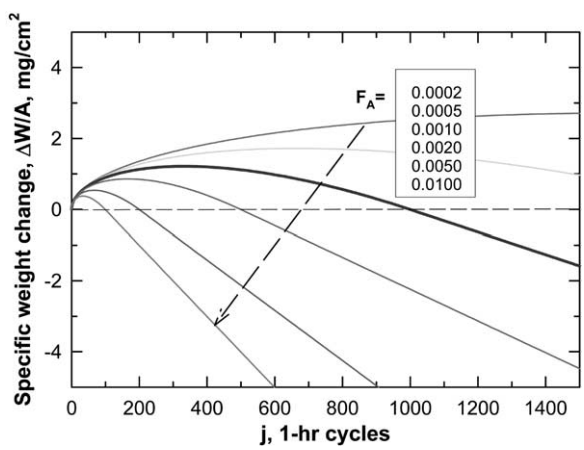

Fig. 7. The effect of spall area fraction, F_A , on the family of DICOSM weight change curves. Baseline value of F_A=0.001 shown as bold line (S_c=2.0, k_p=0.01 mg^2/cm^4 h, Δt=1.0 h).

Fig. 5 shows the effect of increasing the stoichiometric constant from 1.0 to 5.0. The limiting value of S_c=1, (zero cation weight), indicates an upper bound for oxides with low metal contents. The trend with increasing metal content is a downward compression of the entire curve. Most common oxides possess an S_c between 2 and 5, as listed

in Table 2. Al_2O_3, for example, is relatively low at 2.1243, with few oxides below this. Intermediate values are observed for NiO (4.6690) and the spinel $NiAl_2O_4$, (2.7603). Very high values are possible for the heaviest cations, such as ThO_2 (8.2515), or for cation-rich stoichiometry, such as Cu_2O (8.9435).

The effect of increasing the growth product, $k_p\Delta t$, two orders of magnitude from 0.001 to 0.1 is shown in Fig. 6. The curves show a vertical amplification: the maximum in weight gain increases, as does the final linear rate of weight loss, but with no change in cycle number to maximum or zero weight. Note that the effect of increasing cycle duration is equivalent to that of k_p, as indicated by Eqs. (9) and (10), and so both have been combined here into one parameter. But, if only Δt is changed and the family of curves is plotted against total time, they exhibits an upward trend with Δt approaching that of parabolic isothermal oxidation [18].

Table 2
Stoichiometric constant, S_c, (weight of oxide to oxygen) for many common oxides

Row	Atomic number	Oxide	S_c
2	3	Li_2O	1.8675
	4	BeO	1.5633
	5	B_2O_3	1.4500
3	11	Na_2O	3.8738
	12	MgO	2.5191
	13	Al_2O_3	2.1243
	14	SiO_2	1.8777
4	22	TiO_2	2.4959
	23	V_2O_5	2.2736
	24	Cr_2O_3	3.1666
	25	Mn_2O_5	2.3735
	25	Mn_2O_3	3.2892
	26	Fe_2O_3	3.3270
	26	Fe_3O_4	3.6178
	26	FeO	4.4904
	27	CoO	4.6835
	28	NiO	4.6690
	29	CuO	4.9718
	29	Cu_2O	8.9435
5	40	ZrO_2	3.8509
	41	Nb_2O_5	3.3227
	42	MoO_3	2.9988
6	72	HfO_2	6.5780
	73	Ta_2O_5	5.5239
	74	WO_3	4.8301
7	90	ThO_2	8.2515
Mixed	13,14	$Si_2Al_6O_{13}$	2.0484
	13,22	$TiAl_2O_5$	2.2729
	13,39	$AlYO_3$	3.4144
	13,28	$NiAl_2O_4$	2.7603
	24,28	$NiCr_2O_4$	3.5421
	22,28	$NiTiO_3$	3.2201
	28,73	$NiTa_2O_6$	5.3813
	24,41	$CrNbO_4$	3.2642
	24,73	$CrTaO_4$	4.6339
	28,74	$NiWO_3$	4.7897

Fig. 7 presents the trend with increasing the spall (area) fraction, F_A, seen to be similar to that observed for S_c. The downward compression of the entire curve is apparent, but with not as strong a dependence. An upper bound to the curves is defined by F_A=0, i.e., a continuously rising parabolic growth curve. A lower extreme is defined as F_A approaches unity, essentially eliminating the apparent maximum in weight gain and commencing with a linear rate of weight loss.

4. Algebraic approximation and descriptive parameters

This model produced all the characteristic features and trends normally associated with cyclic oxidation weight change curves: an initial maximum, followed by decreasing and eventually negative weight change, and finally a steady-state linear rate of weight loss (concurrent with attaining both a limiting oxide thickness and constant mass fraction of scale spalled each cycle). Trends in these features with input parameters have been demonstrated in previous modeling studies. However, any mathematical descriptions have been indirect, i.e., by trial and error fits to various functions [2] or by regression analysis of the results of many model cases [4]. Indeed, weight change behavior has only been implicitly defined by means of an algorithm or summation series.

4.1. The Good–Smialek approximation

To express the cyclic response curves more explicitly, an attempt was made to find a substi-

tution for the term $\sum\sqrt{i}$ appearing in all the DICOSM functions by Dr. Brian Good and the use of the math program, *Mathematica*©[19]. An expansion in the terms $j^{1/2}$, $j^{2/2}$, $j^{3/2}$, $j^{4/2}$, $j^{5/2}$+K was found, producing the Good approximation (GA):

$$\sum_{1}^{j}\sqrt{i}_{\mathrm{GA}} = aj^{1/2} + bj^{2/2} + cj^{3/2} + dj^{4/2} + ej^{5/2} + K \tag{11}$$

where the coefficients produced by linear regression were identified as: a=0.48957, b=0.0012181, c=0.66660, d=1.8489×10^{-6}, e=−1.90171x10^{-9}, K=−0.169614.

This equation has yielded an extremely accurate expression for any j>10, and a maximum error of only 1.2% at j=1. The excellent agreement over a large range of values for j can be seen in Fig. 8 (as the large open circles). For purposes of subsequent analyses, however, this 6-term function is cumbersome. Thus, because of the small coefficients for three of the terms (b, d, and e), the expression was further simplified, using just a, c, and K, to yield the Good–Smialek approximation (GSA):

$$\sum_{i=1}^{j}\sqrt{i}_{\mathrm{GSA}} \cong \frac{1}{2}j^{1/2} + \frac{2}{3}j^{3/2} \tag{12}$$

Now the error is $16^2/_3$% at j=1, primarily due to ignoring the term K. But this error is quickly reduced to <1% for j<10, and to <0.1% for j>50

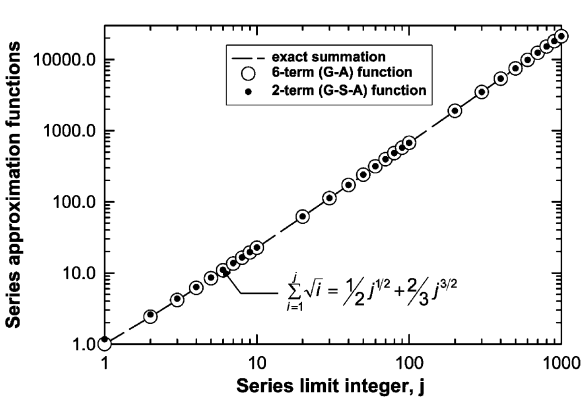

Fig. 8. Comparison of Good–Smialek approximations to $\sum_{i=1}^{j}\sqrt{i}$.

[19]. At j=1000 the error is only 0.001%. Thus, for a reasonable number of cycles corresponding to most tests, the simple expression in Eq. (12) provides an excellent approximation as shown by the small filled circles in Fig. 8.

4.2. Explicit weight change relation.

Substitution of Eq. (12) into the relations for $\Delta W/A$, Eqs. (9) and (10) and all the other output equations (Table 1) yields a new set based on the GSA, where A and B again refer to the portions of the curve where $j \le n_{\mathrm{o}}$ and $j \ge n_{\mathrm{o}}$:

$$(\Delta W/A)_{\mathrm{GSA,\,A}} \cong F_{\mathrm{A}}\sqrt{k_{\mathrm{p}}\Delta t}\left\{\frac{1}{2}(2n_{\mathrm{o}} - S_{\mathrm{c}})(j)^{1/2} + \frac{1}{3}(1-2S_{\mathrm{c}})(j)^{3/2}\right\} \tag{13a}$$

$$(\Delta W/A)_{\mathrm{GSA,\,B}} \cong F_{\mathrm{A}}\sqrt{k_{\mathrm{p}}\Delta t}\left\{\left((1-S_{\mathrm{c}})j - \frac{1}{2}S_{\mathrm{c}}\right)(n_{\mathrm{o}})^{1/2} + \frac{1}{3}(1 + S_{\mathrm{c}})(n_{\mathrm{o}})^{3/2}\right\} \tag{13b}$$

The utility of these new expressions is that the weight change and all the other model outputs can be easily and directly calculated for any particular cycle and any desired combination of the model parameters (S_{c}, k_{p}, Δt, F_{A}, [n_{o}]), as listed in Table 3. No iterative calculations or programmed solutions are required.

The results of the GSA calculations [Eq. (13)] is shown for the baseline model in Fig. 1 as symbols. Note that there is virtually no difference compared to the exact DICOSM calculations (solid line). The numerical data for these two models also shows complete agreement to four decimal places [19]. In fact, it is only in the extreme cases that any differential can be discerned, such as for S_{c}=5 and F_{A}=0.1. Here appreciable errors (25%) have been produced in the first few cycles, but even these diminish to less than 1% in 10 cycles [19]. Thus, the GSA substitution for the DICOSM relations is mathematically robust for most practical cases.

Table 3
List of relations describing DICOSM model outputs using the Good-Smialek Approximation

Cumulative total weight of oxygen or metal reacted:

$$\Sigma W^{GSA}_{oxy,A} = F_A\sqrt{k_p\Delta t}\left\{n_o j^{1/2} + \frac{1}{3}j^{3/2}\right\}$$

$$\Sigma W^{GSA}_{oxy,B} = F_A\sqrt{k_p\Delta t}\left\{j n_o^{1/2} + \frac{1}{3}n_o^{3/2}\right\}$$

$$\sum W^{GSA}_{met} = (S_c-1)\sum W^{GSA}_{oxy}$$

Weight of retained scale, before (W'_r) and after (W_r) spallation:

$$W'^{GSA}_{r,A} = S_c F_A\sqrt{k_p\Delta t}\left\{\left(n_o + \frac{1}{2}\right)j^{1/2} - \frac{1}{3}j^{3/2}\right\}$$

$$W^{GSA}_{r,A} = S_c F_A\sqrt{k_p\Delta t}\left\{\left(n_o - \frac{1}{2}\right)j^{1/2} - \frac{1}{3}j^{3/2}\right\}$$

$$W'^{GSA}_{r,B} = S_c F_A\sqrt{k_p\Delta t}\left\{\frac{1}{2}n_o^{1/2} + \frac{2}{3}n_o^{3/2}\right\}$$

Cumulative total weight of oxide spalled (ΣW_s) after j cycles; Fractional weight of oxide spalled (F_s) on cycle j:

$$\Sigma W^{GSA}_{s,A} = S_c F_A\sqrt{k_p\Delta t}\left\{\frac{1}{2}j^{1/2} + \frac{2}{3}j^{3/2}\right\}$$

$$\Sigma W^{GSA}_{s,B} = S_c F_A\sqrt{k_p\Delta t}\left\{\left(j + \frac{1}{2}\right)n_o^{1/2} - \frac{1}{3}n_o^{3/2}\right\}$$

$$F_{s,A} = \frac{1}{\frac{1}{2} + n_o - \frac{1}{3}j}$$

$$F_{s,B} = \frac{1}{\frac{1}{2} + \frac{2}{3}n_o}$$

Equivalent spall constant from COSP model for $j > n_o$:

$$Q_o = \left\{S_c\sqrt{F_A k_p\Delta t}\left(\frac{1}{2} + \frac{2}{3}n_o\right)^2\right\}$$

4.3. Descriptive parameters

4.3.1. Explicit relations

The various descriptive parameters that define the typical characteristics of a cyclic oxidation curve may now be determined analytically, such as the maximum in weight gain, time to reach maximum and zero weight, and final rate of weight loss. The time to maximum gain is determined by differentiating $(\Delta W/A)_A$ with respect to j in (13a), setting dW/dj equal to zero, and solving for j_{max}. The maximum gain is determined by substituting j_{max} into Eq. (13a). Finally the time to zero weight is determined by setting $(\Delta W/A)_A$ equal to zero and solving for j_o. Note that because only Eq. (13a) was used in these derivations, Eqs. (14)–(16a), apply only to Case A, $j < n_o$.

$$(\Delta W/A)_{GSA,max} \cong \frac{F_A\sqrt{k_p\Delta t}}{3}\left\{\frac{(2n_o - S_c)^{3/2}}{(2(2S_c-1))^{1/2}}\right\} \quad (14)$$

$$j_{max} \cong \frac{2n_o - S_c}{2(2S_c-1)} \quad (15)$$

$$j_{o,A} \cong \frac{3(2n_o - S_c)}{2(2S_c-1)} \quad (16a)$$

$$j_{o,B} \cong \frac{2(S_c+1)n_o - 3S_c}{6(S_c-1)} \quad (16b)$$

It can be seen that the first three relations contain some function of the term $(2n_o - S_c)/(2S_c - 1)$. The ratio of j_o/j_{max} produces a simple integer, equal to exactly 3.0, the ratio produced by the numerical model and close to those found (3.3, 3.3, and 3.4) for Al_2O_3 scales by three previous models [2,4,5].

4.3.2. Trends in characteristic features

Trends in the characteristic features are presented in Figs. 9–11, where the baseline case for S_c=2.0 is shown as a bold curve. The depen-

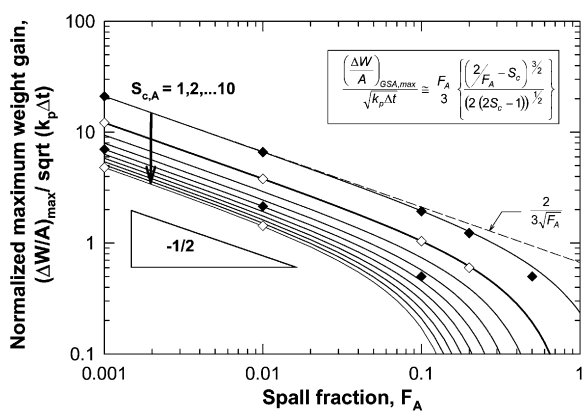

Fig. 9. The effect of spall area fraction, F_A, on the normalized maximum weight change, $(\Delta W/A)_{max}/\sqrt{k_p\Delta t}$, using the GSA solution in the DICOSM model. (Lines refer to GSA solution, symbols refer to actual DICOSM calculations.)

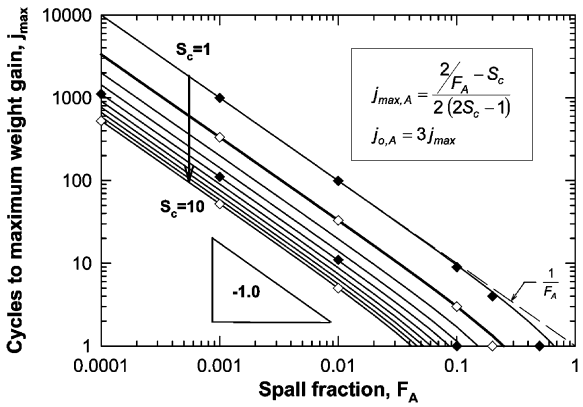

Fig. 10. The effect of spall area fraction, F_A, on the number of cycles, j_{max}, to reach the maximum weight change using the GSA solution in the DICOSM model. (Lines refer to GSA solution, symbols refer to actual DICOSM calculations.)

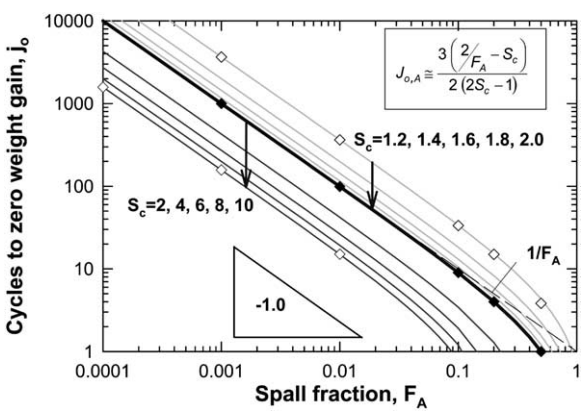

Fig. 11. The effect of spall area fraction, F_A, on the number of cycles, j_0, to reach zero weight change using the GSA solution in the DICOSM model. (Lines refer to GSA solution, symbols refer to actual DICOSM calculations.)

dence of $(\Delta W/A)_{max}$ with S_c and F_A [Eq. (14)] is shown in Fig. 9. Here $(\Delta W/A)_{max}$ is normalized by the term $(k_p\Delta t)^{1/2}$ to collapse the results for all values of the growth product onto one curve. It is seen that $(\Delta W/A)_{max}$ varies nearly as $(F_A)^{-1/2}$ for $F_A \leq 0.1$, i.e., most typical values. A few exact DICOSM calculations [Eq. (9)] are shown as symbols and agree well with GSA results for $F_A \leq 0.1$ in this and the following figures.

The dependence of the number of cycles, j_{max}, to reach maximum weight [Eq. (15)] is shown in Fig. 10. For $F_A \leq 0.1$, j_{max} varies essentially as $(F_A)^{-1}$. Increasing S_c decreases the number of cycles to maximum weight gain. As an extreme example, increasing S_c by a factor of 10 over its theoretical limits of 1 to 10 has the effect of decreasing j_{max} by a factor of ~20.

The same trends are found for the number of cycles, j_o, to reach zero weight, Fig. 11 [Eqs. (16a,b)]. While generally similar to the family of curves for j_{max}, there is one difference that could affect the ratio of j_o/j_{max} and the overall shape of the cyclic oxidation curve. This exception occurs when Case B applies ($j > n_o$) **before** $\Delta W/A$ reaches zero weight change, found by setting $j_{o,B} > n_o$ in Eq. (16b), yielding $S_c \leq 8n_o/(4n_o+3)$. This critical S_c is less than ~2.0 (specifically, 1.860, 1.985, or 1.999 for n_o=10, 100, or 1000, respectively). Conversely, Eq. (16a) (Case A) or (16b) (Case B) must be used to obtain j_o, yielding two sets of curves in Fig. 11 depending on whether $S_c \geq 2$ (lower) or $S_c \leq 2$ (upper), respectively. This special case applies only for SiO_2 (1.878), Li_2O (1.868), BeO (1.563), and B_2O_3 (1.450), Table 2. In terms of the cyclic oxidation curve, this means that a linear terminal slope is reached before the weight reaches zero ($S_c < 2$, Case B). Also the simple ratio of j_o/j_{max}=3 no longer applies because eqn.16a no longer applies.

The final linear slope of the cyclic oxidation curve by differentiating the DICOSM model Eq. (10) [or GSA model Eq.(13b)] with respect to j:

$$\mathrm{TS} = -(S_c - 1)F_A\sqrt{n_o k_p \Delta t} \tag{17}$$

where TS means terminal slope. Since $F_A = 1/n_o$, Eq. (17) can be restated as:

$$\mathrm{TS} = -(S_c - 1)\sqrt{F_A k_p \Delta t} \tag{18}$$

It is therefore apparent that the severity of the final slope increases with S_c, $F_A^{1/2}$, $k_p^{1/2}$, and $(\Delta t)^{1/2}$ on a per cycle basis, or with $(\Delta t)^{-1/2}$ on a per hour basis.

The fractional amount of scale spalled each cycle also reaches a terminal value (Table 1):

$$F_{s,B} = \frac{\sqrt{n_o}}{\sum_{i=1}^{n_o} \sqrt{i}} \tag{19}$$

which is simplified by using the GSA substitution to:

$$F_{s,B} = \left(\frac{1}{2} + \frac{2}{3}n_o\right)^{-1} \cong \frac{3}{2}F_A \quad (20)$$

That is to say that the scale mass fraction spalled per cycle or per hour approaches 1.5 times the area fraction spalled, invariant with scale type, growth rate, or cycle duration.

5. Comparison to other models

These trends are similar to those presented in previous models. An earlier interfacial spalling model also presumed that a constant area fraction spalled to bare metal each cycle [2]. However, instead of biasing the spallation event to only the thickest oxide segment, this model assumed that each new segment also spalls the same area fraction. This leads to an extremely complex model scale structure, with 2^j total segments and correspondingly complex summation equations. However, for most systems of interest, the spall fraction is rarely greater 1% of the area each cycle, such that area of successive spall fractions, $(F_A)^j$ becomes correspondingly minute. It is very similar to the DICOSM model, and similar relations describe the trends in characteristic features [2].

The models described in COSP are more versatile and completely developed [3–5]. This program may simulate spallation from the entire outer surface as a uniform layer or as discrete segments detached at the interface. The latter method involves a randomized probability (Monte Carlo) technique to determine whether a given segment spalls or remains intact (bimodal) on any given cycle. Both methods are governed by one basic formula defining the weight fraction of spalled oxide on a given cycle:

$$F_s = Q_o W'^{\alpha}_r \quad (21)$$

where F_s is the weight fraction of scale spalled, Q_o is a spall constant, W'_r is the weight of intact scale prior to cooling, and the exponent α is a constant, usually taken to be 1.0.

The baseline DICOSM curve is shown as a bold curve in Fig. 12 along with three COSP curves for uniform layer spallation corresponding to the same S_c, k_p and Δt. The first COSP curve was generated so that the cycles to zero weight matched the DICOSM curve. Reasonable agreement occurs up to j_o, but some deviation accrues for the steady state linear loss portion. The second COSP curve was produced by matching the spall fraction, F_s, and shows better agreement in the steady state loss region, but less agreement in the initial portion, $j<j_o$. The third COSP curve has the same final slope as the DICOSM plot, but is offset. These attempts to match the constant spall area fraction model (DICOSM) with the uniform layer spalling model (COSP) produced similar, but not entirely congruent, curves.

This exercise was repeated for the bimodal, interfacial (Monte Carlo) spalling format within COSP. In Fig. 13 two COSP models were adjusted to give the best overall visual fit. One used a Q_o value near those used in the uniform spalling cases. It produced a reasonably close value of j_o and final slope, TS. (Fluctuations in the curve are produced by the randomized Monte Carlo spalling process.) Other attempts used a spall fraction exponent, α, of 0.5 and 0.0 and produced successively better matching with similar output parameters [18]. The DICOSM model appears close to the bimodal COSP model, but without the Monte Carlo varia-

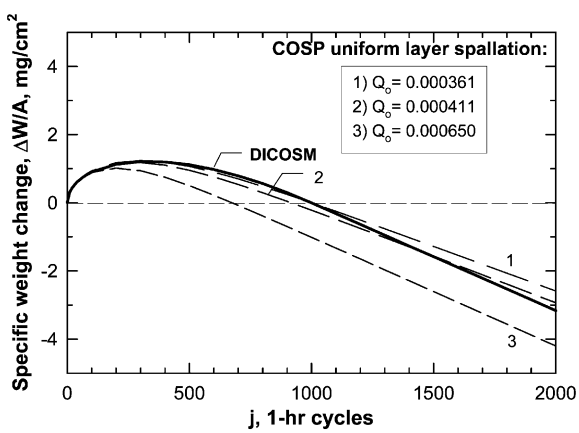

Fig. 12. Matching attempts of three uniform spalling layer COSP model cases to baseline DICOSM curve on the basis of (1) j_o, (2) F_s, and (3) TS (for S_c=2.0, k_p=0.01 mg²/cm⁴ h, Δt=1.0 h).

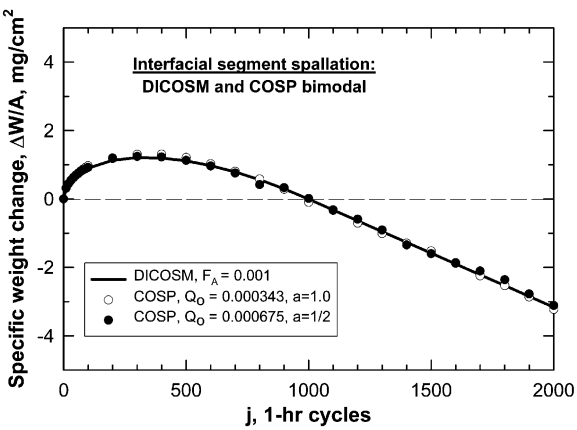

Fig. 13. Matching attempts of two bimodal (interfacial segments) Monte Carlo COSP model cases to baseline DICOSM curve on the basis of the terminal slope, TS (for S_c=2.0, k_p=0.01 mg^2/cm^4 h, Δt =1.0 h).

bility element. These discrepancies are expected from the reported divergence between uniform layer and bimodal spalling configurations [4].

6. Summary

A model for cyclic oxidation has been developed, predicated on parabolic scale growth and a constant area fraction of spallation. Spallation is interfacial and selected only for the thickest segment of intact oxide (deterministic). The weight change behavior can be described by a two-part equation, for the portions where the number of cycles is either less than or greater than the number of area segments. Model curves exhibit typical characteristics: a maximum in weight gain followed by a decrease to zero weight gain and an eventual linear (steady state) rate of weight loss. The effects of stoichiometric constant, parabolic growth rate, spall parameter, and cycle duration all produce regular trends in the response, with reasonable similarities to previous models.

An inherent asset of the present model is its mathematical simplicity. An approximation for the summation series of the square root of an integer was developed and used in DICOSM. It reproduced all the features of the original spalling model with negligible error and enabled the formulation of descriptive parameters as direct functions of the input parameters. Consequently, the maximum weight gain, the number of cycles to reach maximum, the number of cycles to reach zero weight, and the final rate of weight loss may all be calculated directly, allowing for easy analysis of cyclic oxidation data.

Acknowledgements

The many cyclic oxidation model data sets were only made possible by a customized, user-friendly computer program designed by Dr. Judith V. Auping as an adjunct case in our COSP for Windows® product [5]. For this effort I am truly grateful.

References

[1] Barrett CA. A statistical analysis of elevated temperature gravimetric cyclic oxidation data of 36 Ni- and Co-base superalloys based on an oxidation attack parameter. Washington, DC: NASA; 1992. TM-105934.
[2] Smialek JL. Metall. Trans. 1978;9A:309–20.
[3] Lowell CE, Smialek JL, Barrett CA. Cyclic oxidation of superalloys. In: Rapp RA, editor. High temperature corrosion. Houston, TX: NACE 6; 1983. p. 219–26.
[4] Lowell CE, Barrett CA, Palmer RW, Auping JV, Probst HB. Oxid. Met. 1991;36:81–112.
[5] Smialek JL, Auping JV. Oxid. Met. 2002;57:559–81.
[6] Nesbitt JA. In: Romig AD, Dayanada MA, editors. Diffusion analysis and applications. Warrendale, PA: TMS-AIME; 1989. p. 307–24.
[7] Smialek JL, Nesbitt JA, Barrett CA, Lowell CE. Cyclic oxidation testing and modelling: a NASA Lewis perspective. In: Schütze M, Quadakkers WJ, editors. Cyclic oxidation of high temperature materials. London: European Federation of Corrosion, Institute of Materials; 1999. p. 148–68.
[8] Schütze M, Quadakkers WJ, editors. Cyclic oxidation of high temperature materials. London: European Federation of Corrosion, Institute of Materials; 1999.
[9] Evans HE. Int. Met. Rev. 1995;40:1.
[10] Tolpygo VK, Dryden JR, Clarke DR. Acta Mater. 1998;46:927–37.
[11] Wang J-S, Evans AG. Acta Mater. 1998;46:4993–5005.
[12] Tolpygo VK, Clarke DR. Mater. Sci. Eng. 2000;A278:142–50.
[13] Chan KS. Metall. Mater. Trans. 1997;28A:411–22.
[14] Moon CO, Lee SB. Oxid. Met. 1993;39:1–13.

[15] Haynes JA, More KL, Pint BA, Wright IG, Cooley K, Zhang Y. Mater. Sci. Forum 2001;369-372:679–86.
[16] Tolpygo VK, Clarke DR, Murphy KS. Metall. Mat. Trans. 2001;32A:1467–78.
[17] Smialek JL, Pint BA. Mater. Sci. Forum 2001;369-372:459–66.
[18] Smialek JL. A deterministic cyclic oxidation spalling model: part I. Model development and parametric response. Washington, DC: NASA TM, 2002.
[19] Smialek JL. A deterministic cyclic oxidation spalling model: part II. Algebraic approximation, descriptive parameters, and normalized universal curve. Washington, DC: NASA TM, 2002.